doi:10.1093/plcell/koab199

THE PLANT CELL

THE PLANT CELL 2021: 33: 3235–3249

Breakthrough Report

An ABHD17-like hydrolase screening system to identify de-S-acylation enzymes of protein substrates in plant cells

Xiaoshi Liu [1,‡] Min Li [1,‡] Yang Li [1,‡] Zian Chen [1] Chun Zhuge [1] Youwei Ouyang [1] Yawen Zhao [1] Yuxin Lin [1] Qi Xie [2] Chengwei Yang [1,*,†] and Jianbin Lai [1,*,†]

1 Guangdong Provincial Key Laboratory of Biotechnology for Plant Development, School of Life Science, South China Normal University, Guangzhou 510631, China

2 Institute of Genetics and Developmental Biology, Chinese Academy of Sciences, Beijing 100101, China

*Author for correspondence: 20141062@m.scnu.edu.cn (J.L.) and yangchw@scnu.edu.cn (C.Y.).

†Senior authors.

‡These authors contributed equally (X.L., M.L., Y.Li.).

J.L. and C.Y. designed the experiments and supervised the research; X.L., M.L., Y.Li, Z.C., and C.Z. conducted the experiments; Y.O., Y.Z., Y.Lin, and Q.X. provided technological support; J.L. and X.L. analyzed the data and wrote the manuscript.

The author responsible for distribution of materials integral to the findings presented in this article in accordance with the policy described in the Instructions for Authors (https://academic.oup.com/plcell) is: Jianbin Lai (20141062@m.scnu.edu.cn).

Abstract

Protein S-acylation is an important post-translational modification in eukaryotes, regulating the subcellular localization, trafficking, stability, and activity of substrate proteins. The dynamic regulation of this reversible modification is mediated inversely by protein S-acyltransferases and de-S-acylation enzymes, but the de-S-acylation mechanism remains unclear in plant cells. Here, we characterized a group of putative protein de-S-acylation enzymes in *Arabidopsis thaliana*, including 11 members of Alpha/Beta Hydrolase Domain-containing Protein 17-like acyl protein thioesterases (ABAPTs). A robust system was then established for the screening of de-S-acylation enzymes of protein substrates in plant cells, based on the effects of substrate localization and confirmed via the protein S-acylation levels. Using this system, the ABAPTs, which specifically reduced the S-acylation levels and disrupted the plasma membrane localization of five immunity-related proteins, were identified respectively in Arabidopsis. Further results indicated that the de-S-acylation of RPM1-Interacting Protein 4, which was mediated by ABAPT8, resulted in an increase of cell death in Arabidopsis and *Nicotiana benthamiana*, supporting the physiological role of the ABAPTs in plants. Collectively, our current work provides a powerful and reliable system to identify the pairs of plant protein substrates and de-S-acylation enzymes for further studies on the dynamic regulation of plant protein S-acylation.

Introduction

Protein lipidation, which covalently adds lipid molecules to protein targets, plays a critical role in the regulation of protein functions (Jiang et al., 2018). S-acylation, also known as S-palmitoylation, is a critical type of protein lipidation in eukaryotic cells. S-acylation is the covalent attachment of a long chain fatty acid, usually palmitate, onto a cysteine residue of proteins via a thioester bond (Zaballa

Received March 08, 2021. Accepted July 29, 2021. Advance access publication August 2, 2021

and van der Goot, 2018). Due to an increase of protein hydrophobicity via the introduction of fatty acids, S-acylation facilitates the association of proteins with lipid bilayers and contributes to the membrane localization of peripheral proteins. Besides, S-acylation has also been reported in the regulation of trafficking, stability, and activity of target proteins (Linder and Deschenes, 2007). Unlike other types of lipidations, such as myristoylation and prenylation, S-acylation is a reversible biochemical process that is mediated oppositely by protein S-acyltransferases (PATs) and de-S-acylation enzymes. Thus, this type of dynamic modification precisely controls the localization and function of proteins in the cells under different conditions (Lanyon-Hogg et al., 2017).

Protein S-acylation has been well investigated in yeast and mammalian cells, but the molecular function and regulatory mechanism of this modification remain unclear in plant cells (Hemsley, 2020). Through proteomic approaches, hundreds of proteins have been identified as potential S-acylation substrates in Arabidopsis and *Populus trichocarpa* (Hemsley et al., 2013; Srivastava et al., 2016), supporting the notion that S-acylation is globally involved in regulating various processes during plant development and stress responses. For instance, several families of plant proteins in signaling transduction, such as calcineurin B-like proteins and Rho of Plants GTPases are substrates of S-acylation, which mediates their membrane association and subcellular trafficking (Li and Qi, 2017; Feiguelman et al., 2018).

S-acylation is catalyzed by a group of PATs containing a conserved cysteine-rich domain with a DHHC (Asp–His–His–Cys) motif (Mitchell et al., 2006). There are 23 PATs in human cells and most of them have been reported to be associated with diseases, suggesting that the enzymes that regulate S-acylation are important in both physiology and pathology (De and Sadhukhan, 2018). Using a bioinformatics analysis, a variety of homologs of DHHC proteins were identified in different plant species (Yuan et al., 2013). In Arabidopsis, there are 24 PATs with distinct subcellular localizations (Batistic, 2012), and several PAT–substrate pairs have been characterized. For instance, PAT10 mediates the tonoplast localization of calcineurin B-like proteins in salt stress responses (Zhou et al., 2013); PAT13 and PAT14 partially regulate NO Associated 1 in leaf senescence (Lai et al., 2015). However, de-S-acylation enzymes, which remove acyl groups from protein substrates, have been rarely studied in plant cells.

Protein de-S-acylation, the removal of thioester-linked fatty acids from protein substrates, is mediated by enzymes that promote hydrolysis of thioester bonds between proteins and acyl groups. In mammalian cells, there are multiple families of de-S-acylation enzymes, including two acyl protein thioesterases (APT1 and APT2) and an Alpha/Beta Hydrolase Domain-containing Protein 17 (ABHD17) family of hydrolases (Won et al., 2018). APT1 and APT2 were initially identified as de-S-acylation enzymes of G proteins and were further shown to remove acyl groups from many S-acylated substrates in mammalian cells (Lin and Conibear, 2015b). Recent studies have shown that the ABHD17 family of hydrolases is a putative group of de-S-acylation enzymes in mouse, rat, and human cells. ABHD17 proteins enhance de-S-acylation of protein substrates, including postsynaptic density protein 95 and N-Ras, during the regulation of neuron and cancer development (Lin and Conibear, 2015a; Yokoi et al., 2016).

In the current field of plant protein S-acylation studies, a major question that remains to be answered is how protein de-S-acylation occurs in plant cells. In *Medicago falcate*, drought stress induces the translocation of an S-acylated NAC family transcription factor from the plasma membrane to the nucleus, possibly via its de-S-acylation by a thioesterase, which belongs to a group of single hotdog fold fatty acyl-ACP thioesterases, but further biochemical evidence is needed to support the notion that this thioesterase reduces the S-acylation level of its potential substrate (Duan et al., 2017). A maize (*Zea mays*) protein ZmB6T1C9 was predicted as a potential S-acyl protein thioesterase, based on its structural homology to mammalian APTs, but the activity of this maize enzyme and its Arabidopsis homolog TIPSY1 in protein de-S-acylation has not yet been found (Burger et al., 2017). Thus, the de-S-acylation enzymes in plants, even in the model plant Arabidopsis, remain to be functionally characterized.

There are no homologs in plants with high similarity to mammalian APT1 and APT2 (Hemsley, 2020), suggesting that other types of enzymes may catalyze the removal of acyl groups from plant proteins. Although no apparent Arabidopsis proteins with high levels of identity to full-length mammalian ABHD17 proteins, our bioinformatics analysis identified a group of Arabidopsis hydrolases that share a conserved ABHD region with mammalian ABHD17 proteins. Therefore, this group of enzymes (named ABHD17-like Acyl Protein Thioesterases, ABAPTs), including 11 members containing an ABHD with essential residues for catalysis, is potentially involved in protein de-S-acylation in plant cells.

To measure the functions of ABAPTs in plant cells, we tested their actions on the S-acylation of immunity proteins in Arabidopsis. Protein S-acylation has been reported to play an important role in plant immunity responses (Turnbull and Hemsley, 2017), because several key components in pathogen resistance, such as RPM1-Interacting Protein 4 (RIN4; Takemoto and Jones, 2005; Afzal et al., 2011) and AvrPPHB Susceptible1 (PBS1; Qi et al., 2014), have been identified as S-acylation substrates. Besides, our bioinformatics prediction indicated that a couple of immunity-related proteins also harbor potential S-acylation sites. Given that S-acylation is essential for membrane localization of peripheral proteins (Wang et al., 2020), their localization is an obvious marker for de-S-acylation. Therefore, in our current study, we established a robust ABHD17-like hydrolase screening system to identify pairs of substrates and their de-S-acyl enzymes. The enzymes involved in de-S-acylation of five

Arabidopsis immunity proteins were identified for specific reduction of the plasma membrane localization and S-acylation level of their substrates. This functional characterization of ABAPTs will improve our understanding of the dynamic regulation of protein S-acylation in plant cells.

Results

Identification and bioinformatics analysis of a group of ABHD17-like proteins in Arabidopsis

Because APTs have not yet been functionally identified in Arabidopsis, a bioinformatics analysis based on protein BLAST was performed using homologs of ABHD17 family proteins from human, mouse, and rat, which have been recently discovered as protein de-S-acylation enzymes in mammalian cells (Lin and Conibear, 2015a; Yokoi et al., 2016), to identify potential ABHD17-like proteins in Arabidopsis. As a result, 11 proteins with a conserved ABHD region to the mammalian homologs were identified in Arabidopsis (Figure 1A). Thus, these Arabidopsis proteins were named ABAPTs (from 1 to 11, dependent on their protein identity to human/mouse ABHD17B). To illustrate the evolutionary relationship between Arabidopsis ABAPTs and mammalian ABHD17 proteins, a phylogenetic tree was constructed using protein sequences. Given that TIPSY1 was previously proposed to be a potential thioesterase from a structure prediction (Burger et al., 2017), it was used as a control. Compared to TIPSY1, the ABAPT proteins are evolutionarily closer to mammalian ABHD17 proteins (Figure 1B; Supplemental Data Set S1), supporting the notion that these proteins play a similar function in Arabidopsis.

All the ABAPT proteins shared a conserved ABHD region with a high identity (Supplemental Figure S1), but their N- and C-terminal sequences varied among different members. Previous studies indicated that a catalytic triad on the mammalian ABHD17 protein, including a serine, an aspartate, and a histidine residue, is essential for its de-S-acylation activity (Yokoi et al., 2016). These conserved residues were also found in all ABAPTs (Figure 1A), suggesting a similar reaction mechanism exists for plant homologs. For further functional analysis, these *ABAPT* genes were cloned into an overexpression vector and fused with a GFP tag to measure their expression and subcellular localization. The results from confocal microscopy indicated that these ABAPTs were expressed well and distributed globally in plant cells (Supplemental Figure S2), which were suitable for further functional analysis.

Identification of plant immunity proteins as substrates for functional screening of de-S-acylation enzymes

Given that the attachment of fatty acid increases the affinity of protein substrates for lipid bilayers, S-acylation may contribute to membrane localization of proteins. Thus, it will be an easy way to identify de-S-acylation enzymes of target proteins, dependent on the translocation of protein substrates. Given that many immunity-related proteins are localized on the plasma membrane for pathogen sensing and signal transduction, several of them are potential S-acylation substrates in plant cells (Zhou and Zhang, 2020). Five proteins that play important functions in plant immunity were chosen as S-acylation candidates, including RIN4 (Zhao et al., 2021), PBS1 (Swiderski and Innes, 2001), PBS1-Like 1 (PBL1; Ranf et al., 2014), Hypersensitive-Induced Reaction 2 (HIR2; Qi et al., 2011), and Botrytis-Induced Kinase 1 (BIK1; Veronese et al., 2006). Among them, RIN4 and PBS1 have been reported to be S-acylation substrates (Takemoto and Jones, 2005; Qi et al., 2014), but no biochemical evidence has been provided; PBL1, HIR2, and BIK1 also harbor potential S-acylation sites, but they have not yet been functionally characterized as S-acylation substrates.

The potential S-acylation sites of these proteins were predicted using CSS-PALM software (Ren et al., 2008), and the predicted cysteine residues close to the N or C terminus were mutated to serines. Then the wild-type and mutant versions of these candidates were fused with a GFP tag and expressed in Arabidopsis protoplasts for the biotin-switch assay (Hemsley et al., 2008) to confirm the S-acylation and verify modified sites on these immunity proteins in plant cells. The data supported the notion that all five of these proteins were S-acylation substrates, and mutations on the potential modification residues abolished their S-acylation (Figure 1C; Supplemental Figure S3). Concurrently, the subcellular localization of these GFP-tagged substrates was also detected using confocal microscopy. The wild-type of these candidates localized on the plasma membrane, but mutation of S-acylation sites resulted in their translocation into the cytoplasm regions (Figure 1D). These results provided evidence that S-acylation is essential for the localization on the plasma membrane of RIN4, PBS1, PBL1, HIR2, and BIK1. Interestingly, although HIR2 belongs to the HIR family, the members of which contain a putative transmembrane domain embedded within a Band 7-domain (Zhou et al., 2010; Qi et al., 2011), the mutation of S-acylation sites resulted in its distribution into certain structures in the cytoplasm compartment. Thus, these immunity proteins are suitable for screening of their de-S-acylation enzymes, through their translocation when they are co-overexpressed with ABAPTs; and will then be confirmed by the S-acylation levels (Figure 1E).

Systemic screening of ABAPTs to determine de-S-acylation enzymes of the immunity-related protein substrates in plant cells

To establish a screening system to identify ABAPTs that function as de-S-acylation enzymes to target proteins, 11 *ABAPTs* were cloned into an overexpression vector, each fused with a GFP tag at their C terminus. For S-acylation substrates, *RIN4*, *PBS1*, *PBL1*, *HIR2*, or *BIK1* were cloned into an overexpression vector with an RFP tag. In the screening system, a plasmid carrying a distinct RFP-tagged protein substrate was co-transformed into Arabidopsis protoplasts with the empty GFP vector, the *TIPSY1-GFP* control plasmid, or

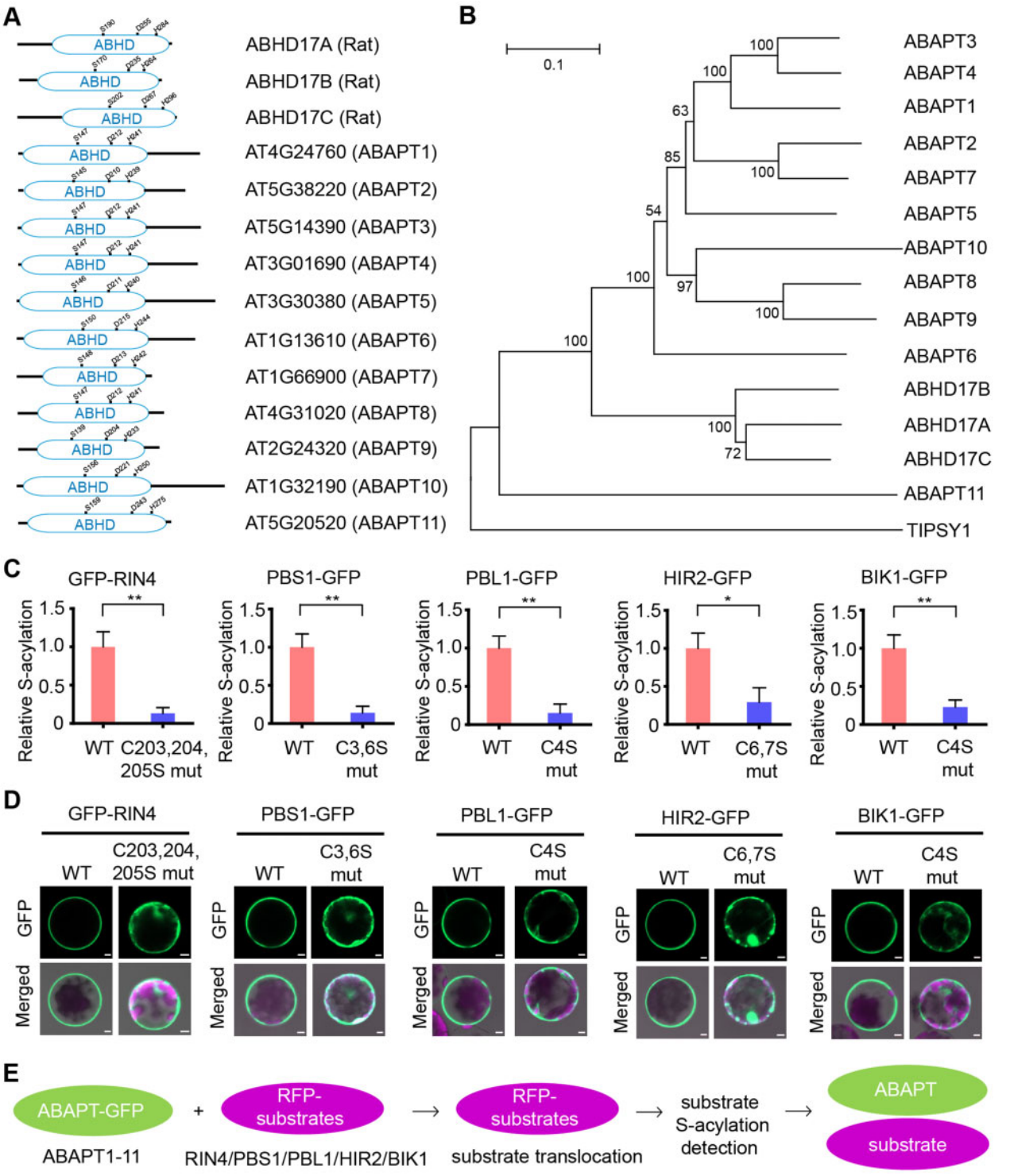

Figure 1 Identification of ABAPT family proteins in Arabidopsis and establishment of a system for screening of de-S-acylation enzymes. A, Domain architecture of the Arabidopsis ABAPT family proteins and rat ABHD17 proteins. The ABHD regions and conserved residues involved in catalysis are indicated. B, Phylogenetic tree of the ABAPT family proteins. The phylogenetic tree was constructed with full-length protein sequences using the neighbor-joining method and tested via bootstrap analysis (1,000 replicates). The scale bar represents genetic distance. The rat ABHD17 proteins and the Arabidopsis TIPSY1 were also included in the analysis. C, Identification of immunity-related protein substrates for the screening of de-S-acylation enzymes. The mutations of predicted S-acylation sites: GFP-RIN4 (C203,204,205S); PBS1-GFP (C3,6S); PBL1-GFP (C4S); HIR2-GFP (C6,7S); BIK1-GFP (C4S). The relative S-acylation levels of the wild-type (WT) and S-acylation site mutant versions of GFP-tagged substrates (RIN4, PBS1, PBL1, HIR2, and BIK1) were measured using a biotin-switch assay. Representative immunoblots are shown in Supplemental Figure S3. The relative S-acylation levels of substrates were calculated from signals ([pulldown+/input+] – [pulldown−/input−]), quantified using ImageJ; the relative S-acylation level of WT substrates is set to 1. The data are mean ± SD from three biologically independent experiments (independent plant growth, independent protoplast transformation, and independent biochemical assays). *P <0.05, **P <0.01, Student's t test

one of the eleven *ABAPT-GFP* plasmids, respectively. When the fluorescent proteins were expressed, the protoplasts with the co-expression of RFP and GFP-tagged signals were used for subcellular analysis (Figure 2).

When co-expressed with the empty GFP protein, the RFP-tagged RIN4 was predominantly localized on the plasma membrane. When co-expressed with most of the ABAPT-GFP proteins or the TIPSY-GFP control, the plasma membrane association of RIN4 was not affected. However, in >50% of cells with the co-expression of ABAPT8-GFP and RFP-RIN4, the translocation of RIN4 into the cytosol was observed (Figure 2A; Supplemental Figure S4A), similar to its localization pattern when S-acylation sites had been mutated. These data implied that ABAPT8 is a potential de-S-acylation enzyme of RIN4. A similar approach was used to identify ABAPTs which specifically remove S-acyl fatty acid from other candidate substrates. As a screening result, ABAPT11-GFP interfered with the plasma membrane of PBS1-RFP (Figure 2B; Supplemental Figure S4B). Surprisingly, the localization of PBL1-RFP was also affected by ABAPT8 (Figure 2C; Supplemental Figure S4C). ABAPT7-GFP resulted in the translocation of the HIR2-RFP proteins into cytosolic compartments (Figure 2D; Supplemental Figure S4D). Similar to the RIN4 and PBL1 proteins, the localization of BIK1-RFP was also affected in the *ABAPT8* overexpressing cells (Figure 2E; Supplemental Figure S4E). The overexpression of ABAPT7, ABAPT8, and ABAPT11 in the transformed protoplasts was confirmed by reverse transcription polymerase chain reaction (RT-PCR; Supplemental Figure S5). To exclude the possibility that the substrates are mislocalized by their overexpression, GFP-RIN4 and PBS1-YFP were expressed under their own native promoters, and the effect of ABAPT8 and ABAPT11 on the subcellular localization of GFP-RIN4 and PBS1-YFP was detected, respectively; the results were consistent with the conclusion from overexpression (Supplemental Figure S6). In summary, these protein substrates were identified as potential targets of the same or different de-S-acylation enzymes in plant cells.

Confirmation of the effect of ABAPTs on the subcellular localization of their targeted substrates

When the potential substrate–ABAPT pair had been identified via co-transformation screening, the genes of the substrate and ABAPT were cloned into two overexpression cassettes in a plasmid, to improve the efficiency of co-expression. Under this situation, the GFP-tagged substrates, including RIN4, PBS1, PBL1, HIR2, and BIK1, were translocalized into the cytosolic regions in the majority of the plant cells with the overexpression of their ABAPTs (Figure 3A), confirming the conclusions from co-transformation.

To confirm that the translocalization of these substrates is mediated by their de-S-acylation enzymes, a cell fractionation assay based on ultra-centrifugation was performed to separate the membrane and soluble fractions. First, the specificity of soluble and pellet fractions of the assay was verified by the free GFP (soluble) and protein acyl-transferase 12 (PAT12), which is a transmembrane protein on the plasma membrane (pellet; Batistic, 2012). After ultra-centrifugation, most of the free GFP was detected in the soluble fraction, and most of the PAT12-GFP was maintained in the pellet fraction (Figure 3B), suggesting that this assay is suitable for further examination. Without the overexpression of ABAPTs, all five selected substrates were predominantly detected in the pellet fraction (Figure 3, C–G), consistent with their localization on the plasma membrane. When co-overexpressed with their specific ABAPT, the majority of GFP-RIN4 (Figure 3C), PBS1-GFP (Figure 3D), PBL1-RFP (Figure 3E), and BIK1-GFP (Figure 3G) accumulated in the soluble fraction, supporting the results from the microscopy observation showing that the translocation of these substrates into the cytosol is mediated by their de-S-acylation enzymes.

Interestingly, the distribution of HIR2-GFP in the pellet fraction was not significantly affected by ABAPT7 (Figure 3F); similarly, the mutation of the S-acylation sites on HIR2 also had no significant effect on its accumulation in the pellet fraction (Supplemental Figure S7); these data are consistent with the previous reports that members of the HIR family harbor a conserved putative transmembrane motif embedded within a Band 7-domain (Zhou et al., 2010; Qi et al., 2011). Thus, the HIR2-GFP that was distributed into the cytosolic compartment upon de-S-acylation may be associated with certain membrane structures. It would be valuable to measure its precise localization in future studies. Taken together, these data indicate that the current screening system is suitable for analyzing protein substrates whose localization is altered by de-S-acylation.

Confirmation of the substrate–ABAPT pairs via measuring S-acylation levels using the biotin-switch assay

The translocalization of substrates may be a result of de-S-acylation, but direct evidence from biochemical assays that measure S-acylation should be provided to confirm the substrate–ABAPT pairs. Compared with the co-transformation assay, the co-expression of the substrate–ABAPT pairs in a

Figure 1 (Continued)

(two-tailed). D, The subcellular localization of the WT and S-acylation defective mutant proteins. The micrographs were taken 36 h after transformation. The GFP signals are in green and the merged images also show chlorophyll autofluorescence in magenta and bright-field in gray (Bars, 5 μm). The images are representatives of three independent experiments (independent plant growth, independent protoplast transformation, and independent microscopy). E, Flow diagram of the screening for de-S-acylation enzymes. The GFP-tagged ABAPT proteins were co-expressed with RFP-tagged substrates (such as RIN4, PBS1, PBL1, HIR2, and BIK1) in protoplasts, and the de-S-acylation enzymes were identified based on localization changes of substrates and confirmed by S-acylation analysis.

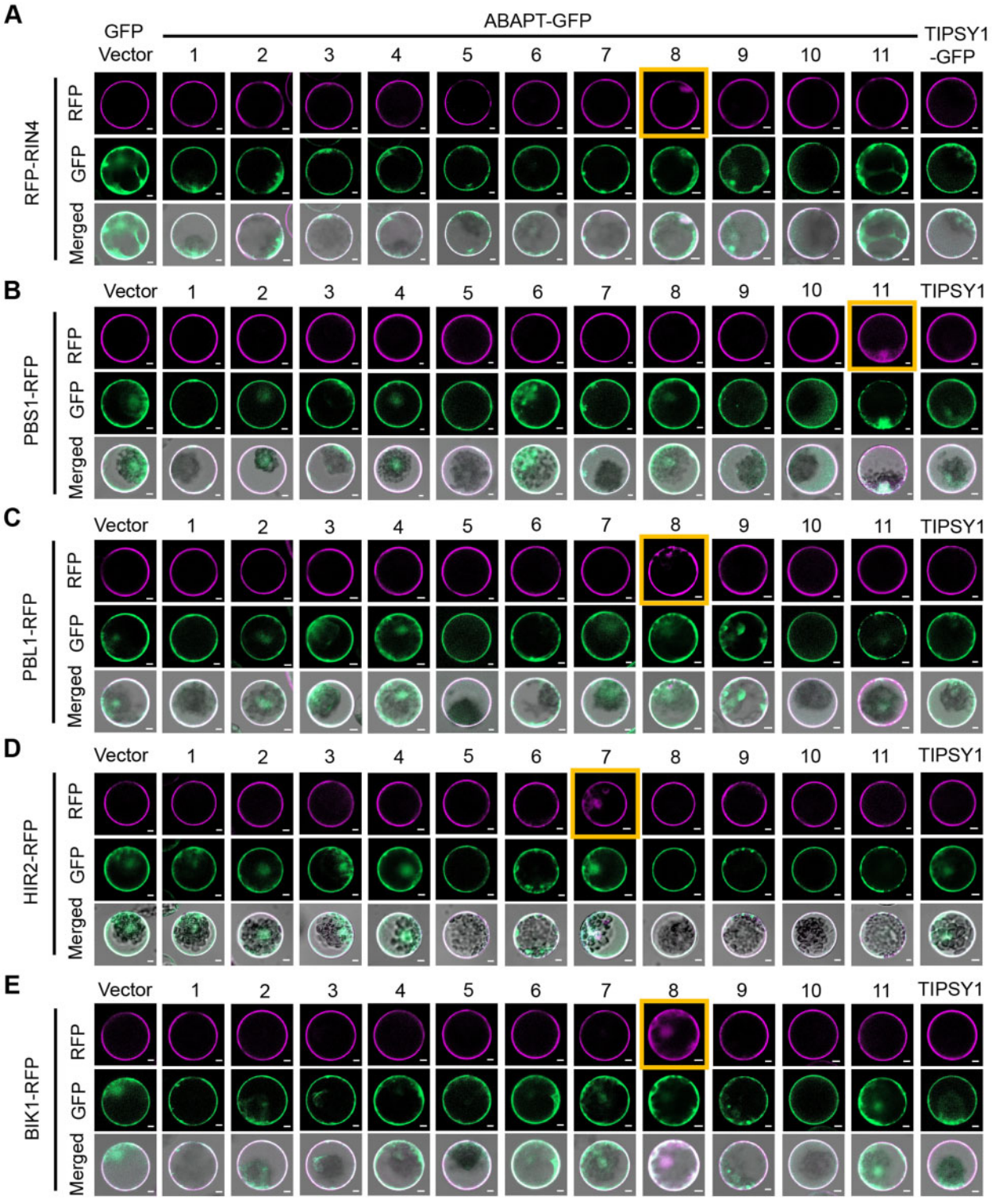

Figure 2 Systemic screening of ABAPTs to determine de-S-acylation enzymes of the immunity-related protein substrates in plant cells. Eleven distinct ABAPT-GFP expressing plasmids were co-transformed with the plasmids expressing RFP-tagged immunity-related protein substrates, respectively. A, RFP-RIN4, (B) PBS1-RFP, (C) PBL1-RFP, (D) HIR2-RFP, and (E) BIK1-RFP. The empty GFP vector and TIPSY1-GFP expressing plasmid were used as controls. The micrographs were taken under confocal microscopy 36 h after transformation. The membrane localization of RFP-tagged substrate proteins was determined from different layers of each cell. The RFP signals (magenta), the GFP signals (green), and the merged images (with bright-field in gray) were recorded. The predominant localization patterns of RFP-tagged substrates (in >50% of cells with both RFP and GFP signals) are shown (Bars, 5 μm). The localization changes of protein substrates are labeled using orange boxes. The images are representatives of three biologically independent experiments (independent plant growth, independent protoplast transformation, and independent microscopy). One hundred cells with both RFP and GFP signals were observed per sample in each independent experiment, and the quantitative data of the percentages of cells with localization changes (distribution into cytosolic regions) are shown in Supplemental Figure S4.

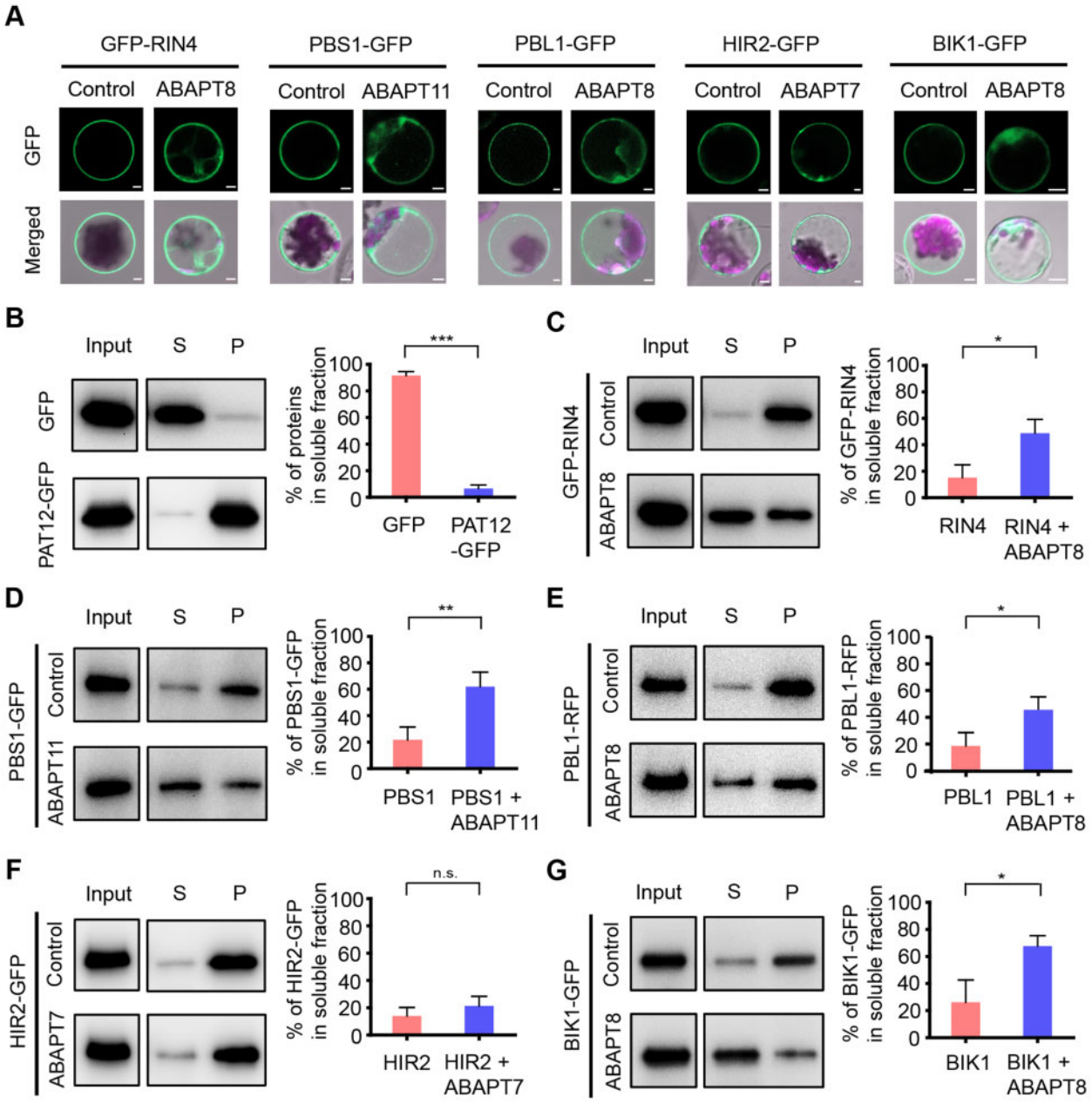

Figure 3 Confirmation of the effect of ABAPTs on the subcellular localization of their targeted substrates. Based on the screening results from Figure 2, the substrate–ABAPT pairs were confirmed via detection of subcellular localization. Both the GFP-tagged substrate gene and its potential *ABAPT* gene were cloned into a vector to improve co-expression efficiency. A, Confirmation of the effect of ABAPTs on the subcellular localization of GFP-tagged substrates using confocal microscopy. Compared to the GFP-tagged substrate alone, which localized on the plasma membrane, the substrates were distributed into the cytosolic regions in the majority of the cells with overexpression of its ABAPT. The GFP signals (green) and merged images (with chlorophyll autofluorescence in magenta and bright-field in gray) are shown (Bars, 5 μm). The images are representatives of three biologically independent experiments. B–G, Measurement of the effect of ABAPTs on substrate localization in a cell fractionation assay. Proteins were expressed in protoplasts and fractionated into soluble (S) and pellet (P) fractions using ultra-centrifugation. B, The specificity of the cell fractionation assay was verified using the free GFP and a transmembrane protein PAT12-GFP as controls for soluble and pellet fractions, respectively. Then the cell fraction distribution of the indicated substrate with or without its ABAPT overexpression was measured. C, GFP-RIN4, (D) PBS1-GFP, (E) PBL1-RFP, (F) HIR2-GFP, (G) BIK1-GFP. As the co-expression of PBL1-GFP with ABAPT8 in a single vector was low, the co-transformation sample of *PBL1-RFP and ABAPT8-GFP* was used instead. The representative images of immunoblots are shown in the left graph. The percentage of substrate proteins in the soluble fraction is shown in the right graph. The immunoblot signals were measured using ImageJ and the percentage was calculated by (S/[S+P]). The data are mean ± SD from three biologically independent experiments (independent plant growth, independent protoplast transformation, and independent biochemical assays). $^{*}P < 0.05$, $^{**}P < 0.01$, $^{***}P < 0.001$, n.s., not significant, Student's *t* test (two-tailed).

plasmid provided an easy and powerful tool for further biochemical analysis.

Using this system, the GFP-tagged RIN4 was expressed with or without ABAPT8 overexpression in Arabidopsis protoplasts, and then the cells were collected for biotin-switch analysis. The free cysteines on proteins were chemically blocked, and then the S-acyl modification was removed from substrates by hydroxylamine (NH_2OH) for exposure of cysteine residues, which further reacted with a biotin-conjugated chemical HPDP; the biotin-labeled proteins were captured by a Streptavidin-Agarose beads, and the enriched substrate proteins were finally eluted using reducing reagents to detect the levels of RIN4 via immunoblotting using an anti-GFP antibody. As a result, the GFP-tagged RIN4 was pulled down on the resins, but the protein level in the pull-down sample was dramatically lower in the presence of ABAPT8 (Figure 4A, left graph). The quantification of three biologically independent experiments supported that ABAPT8 functions as a de-S-acylation enzyme to significantly reduce the S-acylation level of RIN4 (Figure 4A, right graph). Besides, to verify the specificity of the substrate–ABAPT pairs, ABAPT11 was co-overexpressed with GFP-RIN4, but it had no significant effect on the S-acylation level of GFP-RIN4 (Figure 4B; Supplemental Figure S8A), supporting the conclusion that RIN4 is specifically de-S-acylated by ABAPT8. Similarly, the biotin-switch data also confirmed the substrate–enzyme pairs of PBS1-ABAPT11 (Figure 4C; PBS1-ABAPT7 was used as a specificity control [Figure 4D; Supplemental Figure S8B]), PBL1-ABAPT8 (Figure 4E; PBL1-ABAPT11 was used as a specificity control [Figure 4F; Supplemental Figure S8C]), HIR2-ABAPT7 (Figure 4G; HIR2-ABAPT8 was used as a specificity control [Figure 4H; Supplemental Figure S8D]), and BIK1-ABAPT8 (Figure 4I; BIK1-ABAPT11 was used as a specificity control [Figure 4J; Supplemental Figure S8E]). These results supported the conclusion that this screening system is reliable, specific, and suitable for the general screening of de-S-acylation enzymes in plant cells.

Measurement of the mutation effects of three conserved residues essential for the catalytic activity of ABAPT8

Previous studies in mammalian cells showed that three residues in the ABHD region are essential for the hydrolase activity of ABHD17 proteins (Yokoi et al., 2016). Given that these three residues are also conserved in ABAPTs in Arabidopsis, it would be necessary to detect whether these residues are also critical for the activity of ABAPTs. Measurement of the effects of mutations on these residues would answer the question of whether the ABHD17-like proteins from animals and plants share similar catalytic mechanisms.

The pair of RIN4-ABAPT8 was used for further analysis to answer this question. The S147, D212, or H241 on ABAPT8 were mutated to alanine, respectively. RFP-tagged RIN4 was co-expressed with the wild-type, the S147A, the D212A, or the H241A mutant versions of ABAPT8-GFP. The effect of the RFP-RIN4 localization by the wild-type or mutant ABAPT8-GFP was detected using confocal microscopy. In the co-expression cells, the overexpression of the wild-type ABAPT8 lead to translocalization of RFP-RIN4 in >50% of cells, but this effect was almost lost when each residue was mutated (Figure 5, A and B). These data supported the conclusion that all the S147, D212, and H241 residues are essential for the function of ABAPT8. Given that these residues are conserved among ABAPT members, the ABAPT proteins in plant cells may share a similar catalytic mechanism.

Furthermore, the wild-type or triple mutant (all S147, D212, and H241 residues were mutated to alanines) version of *ABAPT8* was cloned into the plasmid overexpressing a GFP-tagged RIN4. Compared with the wild-type ABAPT8, which interfered with the membrane association of RIN4, the triple mutation did not affect the subcellular localization of RIN4 (Figure 5C), confirming that these residues are necessary for the activity of ABAPT8. Consistently, the biotin-switch result showed that the wild-type ABAPT8 dramatically reduced the S-acylation level of RIN4, but the triple mutant had no apparent effects on the RIN4 S-acylation (Figure 5, D and E). Thus, the results from confocal microscopy and the biotin-switch assay supported the conclusion that these three conserved residues in ABHD are essential for the de-S-acylation activity of ABAPT8.

The effect of RIN4 de-S-acylation mediated by ABAPT8 on the level of plant cell death

RIN4 is an important immunity-related factor involved in both pattern-triggered immunity and effector-triggered immunity (Zhao et al., 2021), previous studies indicated that mutation of the S-acylation sites of RIN4 disrupted its localization on the plasma membrane and the overexpression of this mutant version of RIN4 resulted in severe cell death (Afzal et al., 2011). Because we have identified that ABAPT8 is a de-S-acylation enzyme of RIN4, the co-overexpression of ABAPT8 and RIN4 may also lead to cell death.

To test this hypothesis, RFP-RIN4 was transiently expressed in *Nicotiana benthamiana* leaves with or without ABAPT8-GFP. As a result, RFP-RIN4 was localized on the plasma membrane, but this localization was partially interfered with by ABAPT8-GFP (Figure 5F). The translocalization of RFP–RIN4 induced by ABAPT8-GFP was similar to that of its S-acylation defective mutant in *N. benthamiana* leaves. Therefore, the cell death levels of *N. benthamiana* leaves with RIN4 overexpression were compared with or without ABAPT8 via trypan blue staining. Overexpression of RIN4 with the empty GFP vector did not induce apparent cell death, but co-overexpression of RIN4 with ABAPT8-GFP increased the level of cell death, although the level was lower than that in the sample of the S-acylation defective mutant (Figure 5G).

To further confirm the physiological effect of de-S-acylation mediated by ABAPT8, *RIN4* was cloned into *pER8*, an estradiol inducible expression vector (Zuo et al., 2000),

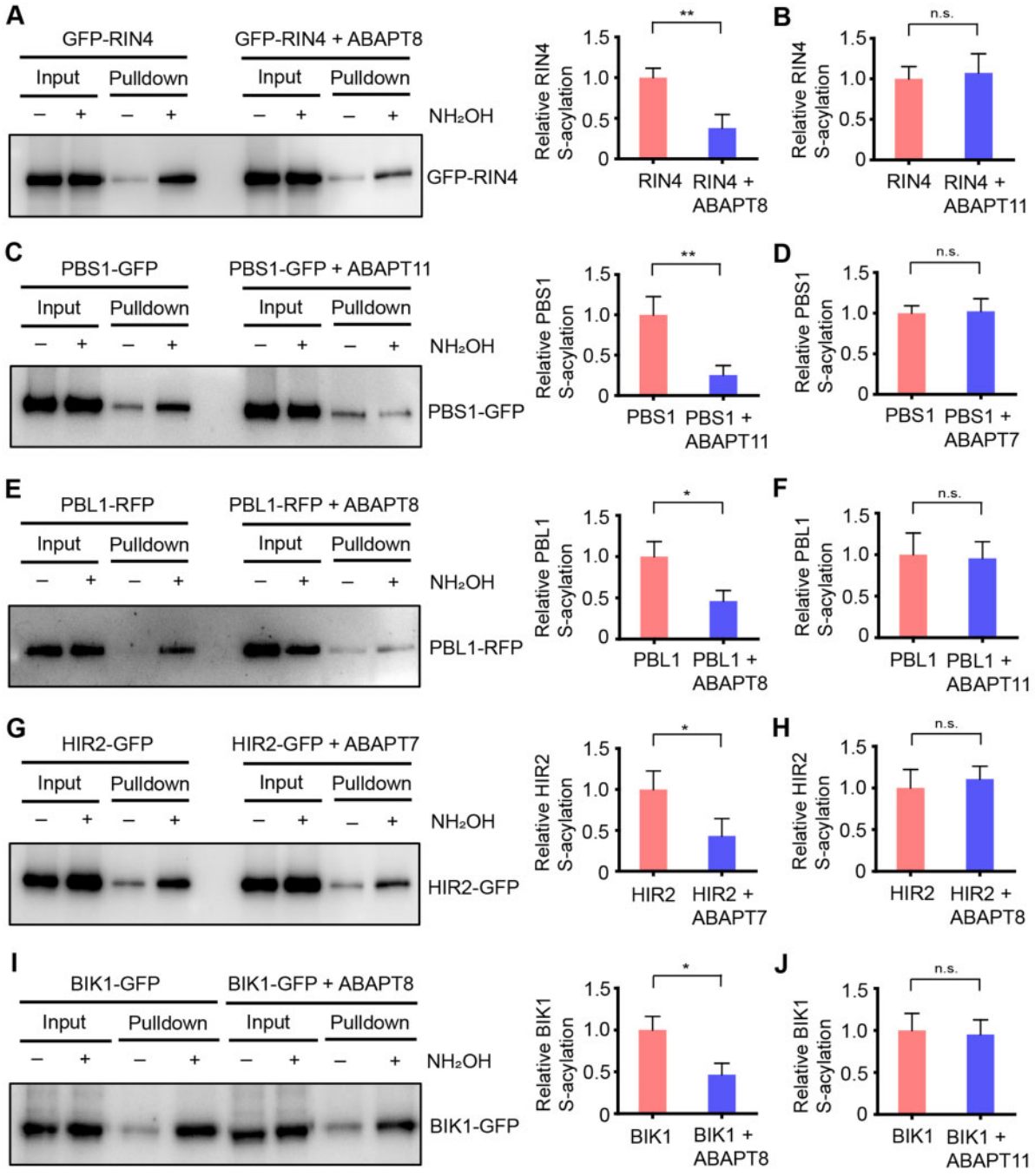

Figure 4 Confirmation of the substrate–ABAPT pairs via measuring S-acylation levels using the biotin-switch assay. The S-acylation levels of GFP-tagged immunity-related substrates with or without the overexpression of its ABAPT were measured using the biotin-switch assay. GFP-RIN4, PBS1-GFP, HIR2-GFP, and BIK1-GFP were co-overexpressed with their ABAPTs in a plasmid, respectively, to improve transformation efficiency. Especially, the co-expression of PBL1-GFP with ABAPT8 in a single vector was low; therefore, the co-transformation sample of *PBL1-RFP and ABAPT8-GFP* was used for S-acylation measurement instead. A, GFP-RIN4 ± ABAPT8; (B) GFP-RIN4 ± ABAPT11 (negative control); (C) PBS1-GFP ± ABAPT11; (D) PBS1-GFP ± ABAPT7 (negative control); (E) PBL1-RFP ± ABAPT8; (F) PBL1-RFP ± ABAPT11 (negative control); (G) HIR2-GFP ± ABAPT7; (H) HIR2-GFP ± ABAPT8 (negative control); (I) BIK1-GFP ± ABAPT8; (J) BIK1-GFP ± ABAPT11 (negative control). The input and pull-down samples with or without NH_2OH were detected using SDS–PAGE and immunoblots. A, C, E, G, and I, The immunoblot images in the left graphs are representatives of three biologically independent experiments. The relative S-acylation levels of substrates with or without its ABAPT overexpression are shown in the right graphs. B, D, F, H, and J, The relative S-acylation levels of substrates with or without a non-specific ABAPT as negative controls. The representative immunoblots of the negative control experiments are included in Supplemental Figure S8. The immunoblot signals were quantified by ImageJ, and the S-acylation levels were calculated from relative signals ([pulldown+/input+] − [pulldown−/input−]); the relative S-acylation level of substrates without ABAPT overexpression is set to 1. The data are mean ± SD from three biologically independent experiments. *P <0.05, **P <0.01, n.s., not significant, Student's t test (two-tailed). All the experiments represented in this figure were performed three times independently (independent plant growth, independent protoplast transformation, and independent biochemical assays).

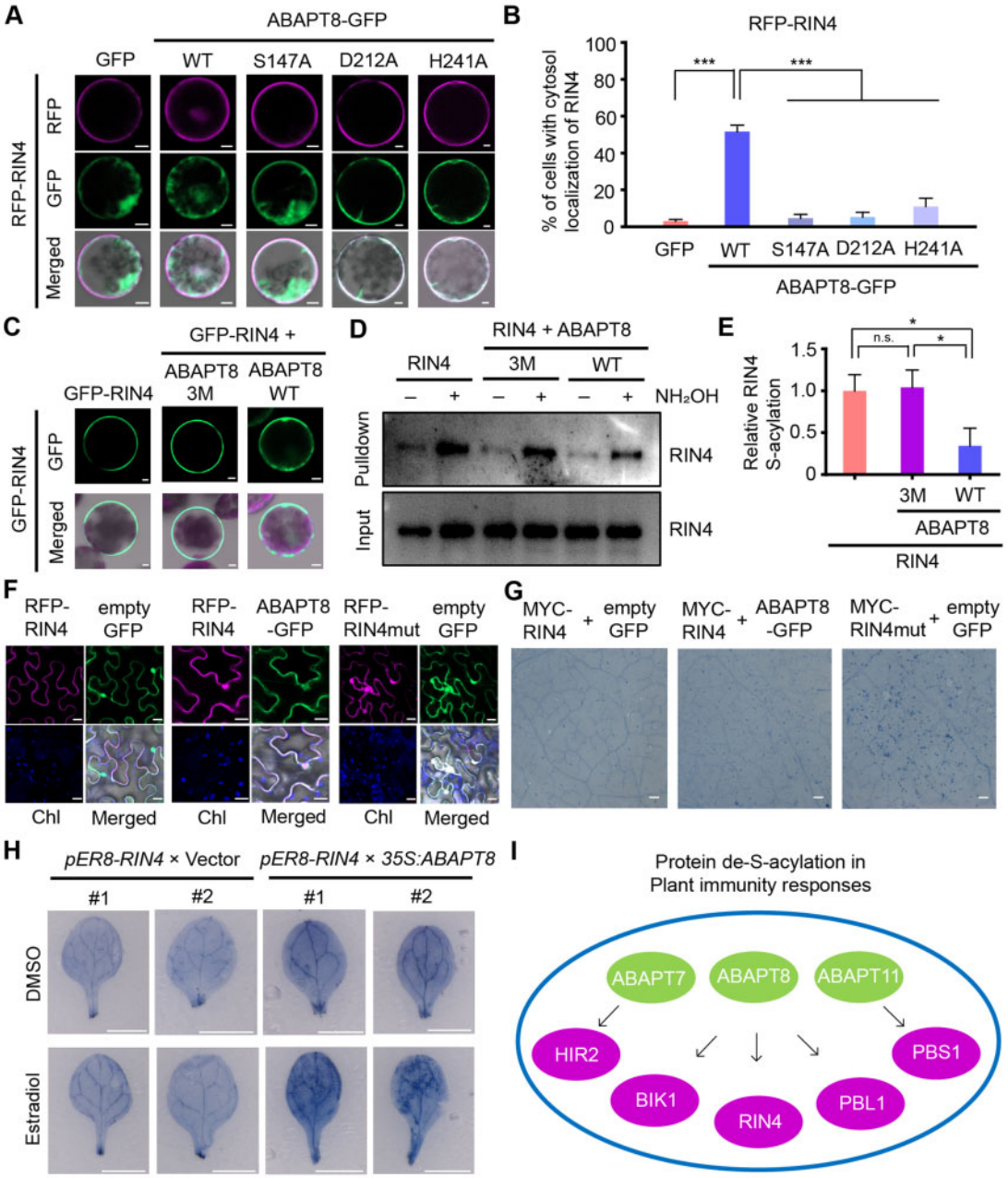

Figure 5 The effects of conserved residue mutations on ABAPT8 activity and the effect of the RIN4 de-S-acylation mediated by ABAPT8 on cell death. A, The effects of co-expression with the wild-type (WT) or the mutant versions of ABAPT8-GFP on the subcellular localization of RFP-RIN4. The RFP signals (magenta), the GFP signals (green), and the merged images (with bright-field in gray) are shown (Bars, 5 μm). The predominant localization patterns of RFP-tagged substrates in >50% of cells with both RFP and GFP signals from three independent experiments are shown. B, The percentages of cells with localization changes of RFP-RIN4 in the presence of the WT and mutant versions of ABAPT8 overexpression. The data are mean ± SD from three independent experiments (at least 100 cells per sample in each experiment). Student's *t* test (two-tailed), ***P <0.001. C, The effect of the ABAPT8 triple mutation (3M: S147A, D212A, and H241A) on the localization of GFP-RIN4. The GFP-tagged *RIN4* was cloned into the same vector with the *ABAPT8* gene to improve co-expression efficiency. The GFP signals (green) and the merged signals (with chlorophyll autofluorescence in magenta and bright-field in gray) are shown. Bars, 5 μm. D, The S-acylation levels of RIN4 with or without ABAPT8 (WT; 3M: S147A, D212A, and H241A) were measured using the biotin-switch assay. The input and pull-down samples with or without NH_2OH were detected using SDS–PAGE and immunoblots. The images are representatives of three biologically independent experiments (independent plant growth, independent protoplast transformation, and independent biochemical assays). E, The relative S-acylation levels of RIN4 with or without ABAPT8 (WT and 3M) were quantified using ImageJ. The values were calculated from relative signals ([pulldown+/input+] – [pulldown–/input–]); the relative S-acylation level of RIN4 alone is set to 1. The data are mean ± SD from three biologically independent experiments *P <0.05; n.s.: not significant; Student's *t* test (two-tailed). F, RFP-RIN4 and ABAPT8-GFP were co-overexpressed in *N. benthamiana* leaves. The S-acylation defective mutant of RIN4 (C203,204,205S) was used as a control. Forty-eight hours after infiltration, the fluorescence was measured. The RFP signals (magenta), the GFP signals (green), the chlorophyll autofluorescence (Chl: blue), and the merged signals (with bright-field

and transformed into Arabidopsis to generate stable transgenic plants. Furthermore, *ABAPT8* was cloned into a *35S:GFP* vector to generate *35S:ABAPT8-GFP* plants. The co-expression plants were generated via genetic crossing between the *pER8-RIN4* and *35S:ABAPT8-GFP* plants. The *35S:GFP* vector transgenic plants were also used as a control during the crossing. The homologous co-transgenic plants were used for further analysis with or without estradiol induction (Supplemental Figure S9). When *RIN4* was induced by estradiol, obvious cell death was observed via trypan blue staining in the leaves co-overexpressing RIN4 and ABAPT8, but not in the control samples (Figure 5H). As a control, the trypan blue staining of the leaves of *35S:ABAPT8-GFP* plants indicated that overexpression of ABAPT8 alone was not enough to result in obvious cell death (Supplemental Figure S10). These data provided evidence that de-S-acylation of overaccumulated RIN4 mediated by ABAPT8 stimulated cell death, confirming our screening of the RIN4–ABAPT8 pair and implying that ABAPT8 may play important functions in the regulation of immunity responses in plants.

Discussion

S-acylation is an important reversible protein modification, but the de-S-acylation mechanism in plant cells remains unknown (Hemsley, 2020). Here, we uncovered a group of ABHD17-like hydrolases and studied their functions in the de-S-acylation of protein substrates, providing a useful system to discover protein de-S-acylation enzymes in plant cells.

In mammalian cells, APT1/2 and ABHD17 are two major types of de-S-acylation enzymes (Won et al., 2018). Given that no apparent homolog of APT1/2 was identified in plants (Hemsley, 2020), the possibility remained that enzymes with low protein identities catalyze similar reactions, because proteins containing low levels of amino acid identities may have similar 3D structures. For instance, the maize protein Zm6T1C9 has structural homology to human APT2, but no biochemical evidence has been provided for its de-S-acylation activity on protein substrates (Burger et al., 2017). TIPSY1, the homolog of ZmB6T1C9 in Arabidopsis, is used as a control in our current study, but no protein target has been identified for this potential thioesterase. Similarly, there is no highly conserved ABHD17 homolog in plants, but here we identified a group of ABAPTs containing a conserved ABHD 17-like region, which is required for the removal of acyl groups from protein substrates (Lin and Conibear, 2015a; Yokoi et al., 2016), although their N- and C-terminals are varied. Our biochemical results showed that mutation of three conserved residues in ABHD significantly reduces the enzyme activity of ABAPT8, suggesting that this family of enzymes has a similar catalytic mechanism as the mammalian ABHD17 proteins. Although the ABHD regions are highly similar among ABAPTs, variation in certain enzymes may contribute to their activity regulation (Supplemental Figure S1). This discovery of functional ABAPTs will provide important enzyme resources for future studies on dynamic plant protein S-acylation. Furthermore, a recent study showed that ABHD10, another human ABHD hydrolase in the mitochondria, is also a de-S-acylation enzyme (Cao et al., 2019); thus, it would be valuable to measure whether other types of plant ABHD proteins also function in protein de-S-acylation.

Based on the identification of the ABAPT family in Arabidopsis, we established a robust system for screening substrate–de-S-acylation enzyme pairs. Given that many S-acylation substrates that have been identified in plant cells are peripheral proteins, this modification is essential for correct membrane localization of target proteins, providing a good marker for general de-S-acylation enzyme screening. Using this approach, the specific de-S-acylation enzymes of five immunity-related proteins have been identified in our current study, suggesting that this system is powerful for further screening of de-S-acylation enzymes of other protein substrates. This system provides a fast and simple tool for plant de-S-acylation studies in any laboratory. The screening could be completed in a week (including protoplast transformation, subcellular observation, and biochemical confirmation); furthermore, no specialized equipment or expertise is needed in this system (other than the ability to perform standard plant culture methods, confocal microscopy, and biotin-switch, which is a specific type of pull-down assay). However, there are some points for attention during using this system. For transmembrane S-acylated proteins whose localization is not obviously affected by de-S-acylation, such as Flagellin Sensing 2 (FLS2; Hurst et al., 2019), the enzyme–substrate pair cannot be identified through the effect on subcellular localization; instead, the biotin-switch assay must be used for direct comparison of the S-acylation levels among samples with different ABAPTs. However, for the

Figure 5 (Continued)

in gray) are shown (Bars, 20 μm). The data are representatives of three independent experiments. G, *MYC-RIN4* was co-expressed with ABAPT8-GFP or GFP using agrobacteria based infiltration in the leaves of *N. benthamiana*. The S-acylation defective mutant of RIN4 (C203,204,205S) was used as a control. Four days after infiltration, the leaves were collected for trypan blue staining to measure the levels of cell death. Bars, 0.5 mm. The data are representatives from three biologically independent experiments. H, The genetic crossing was performed between *pER8-RIN4 and 35S:ABAPT8-GFP* or *35S:GFP* plants. The homozygous off-springs were treated with or without estradiol, an inducer of *RIN4* overexpression. After a 2-day treatment with 20-μM estradiol or DMSO (negative controls), leaves were collected for trypan blue staining. The trypan blue staining of *35S:ABAPT8-GFP* Arabidopsis is shown in Supplemental Figure S10. The data are representatives from three biologically independent experiments (Bars, 5 mm). All the phenotype analyses in this figure are representative of at least three independent experiments (independent plant growth and independent trypan blue staining) with similar patterns. I, Summary of the screening of de-S-acylation enzymes of plant immunity-related substrates in our current work, including the pairs of ABAPT8–RIN4, ABAPT8–PBL1, ABAPT8–BIK1, ABAPT7–HIR2, and ABAPT11–PBS1.

transmembrane proteins whose trafficking is regulated by S-acylation, such as HIR2 used in our current study, this type of transmembrane proteins are suitable for screening via translocalization observation. For the protein substrates whose precise plasma membrane localization is affected by overexpression, a native promoter can be used to express a native level of protein in the screening system. Besides, there may be functionally redundant ABAPTs, which share one protein substrate; in such cases, each enzyme would be able to change the substrate localization, and all the ABAPTs would need to be analyzed carefully to avoid missing any of them. Therefore, redundant ABAPTs can also be identified distinctly using this approach for further functional analysis of multiple enzymes.

S-acylation has been reported to be important in the control of plant immunity factors (Turnbull and Hemsley, 2017), but the dynamic regulation via de-S-acylation is unknown. Here we identified de-S-acylation enzymes of five immunity-associated proteins in plant cells, providing abundant resources for further detailed studies. Our data indicated that ABAPT8 enhances the translocation of RIN4, resulting in cell death in *N. benthamiana* and Arabidopsis leaves, supporting the physiological function of ABAPT8 in plants, but the precise functions of these identified ABAPTs remain to be investigated. Interestingly, our screening data showed that ABAPT8 targets RIN4, PBL1, and BIK1, suggesting this de-S-acylation enzyme has multiple immunity substrates; while identification of the pairs of ABAPT7–HIR2 and ABAPT11–PBS1 indicated the enzyme specificity of different protein substrates (Figure 5I). This specificity may be dependent on the subcellular localization or substrate–enzyme association (Azizi et al., 2019). The ABAPT enzymes seem to be distributed generally in cells, but their precise subcellular localization, possibly expressed under their native promoters, needs to be illustrated in further studies. Because the N- and C-terminals of the ABAPTs (out of the ABHD) vary among the members of this enzyme family, these regions may also contribute to substrate specificity. The majority of these immunity proteins are localized to the membrane, suggesting most of these substrate proteins are constitutively S-acylated in plant cells; thus, it is possible that the expression of de-S-acylation enzymes is low under normal conditions, but may be induced for de-S-acylation under certain conditions (Lanyon-Hogg et al., 2017), such as biotic and abiotic stresses. Therefore, it is important to detect the S-acylation level of these immunity proteins under different environments, and further analyze the phenotypes of the loss-of-function mutants and overexpression lines of the indicated ABAPTs under these situations.

Collectively, we established an ABAPT screening system for the identification of de-S-acylation enzymes of protein substrates in Arabidopsis. This screening system can be used to identify de-S-acylation enzymes of other protein substrates involved in various biological processes in plant cells. Although the current system is based on ABAPTs in Arabidopsis, similar approaches can be used in any other plant species to explore the dynamic regulation mechanisms of protein S-acylation.

Materials and methods

Plant materials and growth conditions

Arabidopsis thaliana seeds of *Columbia-0* were surface sterilized and plated on Murashige and Skoog medium with 1.5% sucrose and 0.8% agar. After stratification at 4°C in the dark for 2 days, the plates were moved to long-day conditions (16-h of light/8-h of dark, 80 μE s^{-1} m^{-2} light intensity provided by white light fluorescent tubes [Philips]) at 22°C for plant growth. Around 1 week after germination, seedlings were transferred to soil for further growth.

Plasmid constructions

For the transient expression of ABAPT-GFP proteins, the indicated genes were cloned into a *pCambia-35S:GFP* expression vector, in which their C terminus (without their stop codons) was fused with a GFP tag. For RFP-tagged substrate proteins, *RIN4* was cloned into a *pCanG:RFP* expression vector, in which an RFP protein was fused to the N terminus of RIN4; *PBS1*, *PBL1*, *HIR2*, or *BIK1* was constructed in a *pCambia1300-UBQ:RFP* expression vector, in which the C terminus of substrates (without their stop codons) was fused with an RFP.

For the biotin-switch assay, both substrate and its *ABAPT* were constructed into *pCambia1302*, in which the substrate was fused with GFP (for RIN4, a GFP tag was fused to its N terminus; for other substrates, GFP was fused to their C terminus [without their stop codons]), while *ABPAT* was used to replace the *Hygromycin* (*R*) gene in the vector, resulting in the co-overexpression of the substrate and its enzyme in a plasmid. Site-directed mutagenesis was used to generate the S147A, D212A, H241A, and triple mutants of ABAPT8.

To examine the effect of an S-acylation site mutation on the localization and S-acylation of protein substrates, the wild-type and mutant versions were cloned into a *pCambia1300-UBQ:GFP* expression vector. Because the S-acylation sites were located at the N or C terminus of substrates, the mutations were introduced from the primers.

For phenotype analysis of transient expression in *N. benthamiana* leaves, *RIN4* was cloned into the *pCanG:MYC* vector, in which its N terminus was fused with a MYC tag. For the inducible expression of *RIN4* in Arabidopsis, *RIN4* was constructed into the *pER8* vector (Zuo et al., 2000).

To express the native levels of RIN4 and PBS1, their own promoter regions were fused with *GFP-RIN4 and PBS1-YFP*, respectively, and cloned into the expression vector *pCambia1300-221* without the *35S* promoter.

The sequence information of the primers used in this study is included in Supplemental Table S1.

Protoplast transformation and confocal microscopy

The protoplasts were prepared from rosette leaves of 3-week-old Arabidopsis plants grown in the soil. The plasmids overexpressing the substrates or ABAPTs fused with

fluorescent proteins were transformed into protoplasts for transient expression as previously described (Yoo et al., 2007). Incubation for 36 h after transformation, the protoplasts were observed under a Zeiss LSM 800 laser-scanning confocal microscope, and the fluorescent signals (RFP or GFP), chlorophyll autofluorescence, bright field, and merged signals were recorded.

Cell fractionation assay

Protoplasts expressing GFP- or RFP-tagged substrates with or without ABAPTs were collected for the cell fractionation assay as previously described (Li et al., 2018) with minor modifications. The cells were re-suspended in a homogenization buffer (50-mM Tris–HCl, pH 7.4, 150-mM NaCl, 1-mM EDTA, 13% sucrose, with a protease inhibitor cocktail) and incubated for 30 min at 4°C. Then the samples were centrifugated at 6,000*g* for 10 min twice at 4°C to remove cellular debris. The supernatants were ultra-centrifugated at 80,000*g* at 4°C for 1 h to obtain soluble and pellet fractions. The pellet was re-suspended in the same volume of homogenization buffer. The soluble and pellet fractions were then used for sodium dodecyl sulphate–polyacrylamide gel electrophoresis (SDS–PAGE) and immunoblot.

Biotin-switch assay

The biotin-switch assay was performed following the protocol previously described (Hemsley et al., 2008) with modifications. In particular, the indicated plasmids expressing GFP-tagged substrates with or without their ABAPTs were transformed into protoplasts. 24 h after transformation, the protoplasts were collected for protein extraction in lysis buffer (25-mM HEPES, 2-mM TCEP, 1-mM EDTA, pH 7.5, and 1× protease inhibitor cocktail). After incubation at 50°C for 5 min, equal volumes of proteins were diluted in blocking buffer (100-mM HEPES, 1-mM EDTA, 2.5% SDS, 0.5% MMTS, pH 7.5) and incubated for 10 min at 40°C with frequent vortexing. Then the samples were mixed with three volumes of cold acetone for protein precipitation at −20°C overnight. The protein precipitates were collected via centrifugation at 5,000*g* at 4°C for 10 min, and the pellets were rinsed using 70% acetone. The pellets were further dissolved in 200 μL of resuspension buffer (8 M urea, 2% SDS, 1× PBS pH 7.4), and the suspension was divided into two tubes (100 μL each). In each tube, 50 μL of 4-mM biotin-HPDP (APExBIO), 2 μL of 100-mM EDTA, and 1 μL of 100× protease inhibitor cocktail were added, with 50 μL of 1-M NH_2OH (pH 7.4; for the removal of S-acyl group) or 1 M-Tris–HCl (pH 7.4; negative control). The mixtures were incubated at room temperature for 1 h, and then mixed with 600 μL of methanol, 200 μL of chloroform, and 800 μL of water, and spun at 10,000*g* at room temperature for 30 min. After the removal of the upper layer, 800 μL of methanol was added. The mixture was placed at −20°C for 20 min and then centrifuged at 5,000*g* at room temperature for 20 min. After removal of the supernatant, the pellet was dried for 10 min at room temperature. Then the pellet was dissolved again in 100 μL of resuspension buffer. Twenty microliters of the resuspension was used as input in immunoblotting, and the rest was diluted with 720 μL of PBS containing 0.2% Triton X-100, and incubated with prewashed Streptavidin-Agarose beads (Sigma) for 1.5 h at room temperature. After incubation, the beads were rinsed sequentially with wash buffer (500-mM NaCl, 0.1% SDS, 1× PBS, pH 7.4) and 1× PBS (pH7.4). Seventy microliters of wash buffer containing 5% β-mercaptoethanol was mixed with the beads for 20 min to elute the S-acylated proteins. After the beads were spun down, the supernatant was mixed with protein sample buffer and heated at 95°C for 5 min for further regular SDS–PAGE and immunoblotting using an anti-GFP antibody (TransGen Biotech, HT801), an anti-RFP antibody (Biodragon B1153), and an anti-mouse secondary antibody (Cell Signaling Technology, 7076S).

Subcellular localization analysis in *N. benthamiana* leaves

35S:RFP-RIN4 and *35S:ABAPT8-GFP* were transformed into agrobacteria *GV3101*, respectively. Forty-eight hours after infiltration in the leaves of *N. benthamiana* as previously described (Liu et al., 2012), the leaves were collected for observation of protein subcellular localization under a Zeiss LSM 800 laser-scanning confocal microscope.

RT-PCR

RNA was extracted from seedlings or protoplasts using the Plant RNAprep Pure Kit (Magen) with DNase I treatment following the manufacturer's instructions. The RNA was used for reverse transcription via a PrimeScript RT Reagent Kit (Vazyme). The cDNA was then used as template in a regular PCR reaction. *ACTIN1* was used as an internal control. The sequences of RT-PCR primers are included in Supplemental Table S1.

Cell death analysis

pCANG-MYC-RIN4 and 35S:ABAPT8-GFP were transformed into agrobacteria *GV3101*, respectively. The transient expression was performed via infiltration in the leaves of *N. benthamiana* as previously described (Liu et al., 2012). Four days after infiltration, the leaves were collected for Trypan blue staining (1:1:1:1 mix of phenol, lactic acid, glycerin, and water plus 0.05% [w/v] trypan blue). After incubation at 95°C for 1 min, 15-M chloral hydrate solution was used for destaining (Koch and Slusarenko, 1990).

The transgenic Arabidopsis plants of *pER8-RIN4*, *35S:GFP*, and *35S:ABAPT8-GFP* were generated via the floral-dip method (Clough and Bent, 1998). More than 10 individual transgenic lines of each genotype (verified by RT-PCR) were obtained with similar phenotypes, and two independent homozygous lines were used for further analysis. The genetic crossing was performed between *pER8-RIN4* and *35S:ABAPT8-GFP* or *35S:GFP* (the vector control) plants, and the homozygous off-spring were used for Trypan blue staining as described above.

Bioinformatics analysis

The protein sequences of Arabidopsis ABAPTs and rat ABHD17A/B/C, which were obtained from the NCBI database, were analyzed via ClustalW, and then the phylogenetic tree was constructed by MEGA7 (Kumar et al., 2016), using the neighbor-joining method, and tested via the bootstrap method (1,000 replicates). To identify the ABHD regions on ABAPTs, their protein sequences were subjected to domain prediction using Interpro (https://www.ebi.ac.uk/interpro/; Apweiler et al., 2000). S-acylation sites were predicted using CSS-PALM (Ren et al., 2008).

Statistical analysis

The data are mean ± SD from three biologically independent experiments (independent plant growth, independent protoplast transformation, and independent microscopy or biochemical assays). The significance analysis was performed using a Student's *t* test (two-tailed) in GraphPad Prism 5. $^{*}P < 0.05$, $^{**}P < 0.01$, $^{***}P < 0.001$, n.s., $P > 0.05$. The *P*-values of statistical analysis in the figures are included in Supplemental Table S2.

Accession numbers

The sequence data from this work can be found in the Arabidopsis Information Resource database (TAIR) or the NCBI database under the following accession numbers: *ABAPT1* (*AT4G24760*); *ABAPT2* (*AT5G38220*); *ABAPT3* (*AT5G14390*); *ABAPT4* (*AT3G01690*); *ABAPT5* (*AT3G30380*); *ABAPT6* (*AT1G13610*); *ABAPT7* (*AT1G66900*); *ABAPT8* (*AT4G31020*); *ABAPT9* (*AT2G24320*); *ABAPT10* (*AT1G32190*); *ABAPT11* (*AT5G20520*); *TIPSY1* (*AT4G22300*); *RIN4* (*AT3G25070*); *PBS1* (*AT5G13160*); *PBL1* (*AT3G55450*); *HIR2* (*AT3G01290*); *BIK1* (*AT2G39660*); *PAT12* (*At4g00840*); Rat *ABHD17A* (GeneID: 299617); Rat *ABHD17B* (GeneID: 309399); Rat *ABHD17C* (GeneID: 361601).

Supplemental data

The following materials are available in the online version of this article.

Supplemental Figure S1. The alignment of ABHDs from ABAPTs and mammalian ABHD17 proteins.

Supplemental Figure S2. The expression of ABAPT-GFP proteins in Arabidopsis protoplasts.

Supplemental Figure S3. The detection of S-acylation of the wild-type and predicted S-acylation site mutation versions of immunity proteins.

Supplemental Figure S4. The percentages of cells with localization changes of substrates in the systemic screening of ABAPTs.

Supplemental Figure S5. Detection of the overexpression of *ABAPT7*, *ABAPT8*, and *ABAPT11* in protoplasts.

Supplemental Figure S6. The effect on the subcellular localization of RIN4 and PBS1 expressed under their native promoters by the identified ABAPTs.

Supplemental Figure S7. Comparison of the membrane distribution of the wild-type and C6,7S mutant versions of HIR2-GFP in a cell fractionation assay.

Supplemental Figure S8. The specificity of the ABAPT–substrate pairs was verified by nonspecific ABAPTs.

Supplemental Figure S9. The transcript levels of *ABAPT8* and inducible *RIN4* in transgenic Arabidopsis plants.

Supplemental Figure S10. Trypan blue staining of the leaves of Arabidopsis plants transgenically overexpressing *ABAPT8*.

Supplemental Table S1. Primers used in this study.

Supplemental Table S2. The *P*-values of statistical analyses in the figures.

Supplemental Data Set S1. Alignments used to generate the phylogeny shown in Figure 1B.

Acknowledgment

We would like to thank Prof. Nam-Hai Chua (Rockefeller University) for kindly providing us with the *pER8* vector.

Funding

This work was supported by the Major Program of Guangdong Basic and Applied Research (2019B030302006), the National Natural Science Foundation of China (31970531, 31771504 and 31871222), the Guangdong Special Support Program of Young Top-Notch Talent in Science and Technology Innovation (2019TQ05N651), the Natural Science Foundation of Guangdong (2018B030308002, 2021A1515011151), the Guangdong YangFan Innovative and Entrepreneurial Research Team Project (2015YT02H032), and the Program for Changjiang Scholars.

Conflict of interest statement. None declared.

References

Afzal AJ, da Cunha L, Mackey D (2011) Separable fragments and membrane tethering of Arabidopsis RIN4 regulate its suppression of PAMP-triggered immunity. Plant cell **23**: 3798–3811

Apweiler R, Attwood TK, Bairoch A, Bateman A, Birney E, Biswas M, Bucher P, Cerutti L, Corpet F, Croning MD, et al. (2000) InterPro–an integrated documentation resource for protein families, domains and functional sites. Bioinformatics **16**: 1145–1150

Azizi SA, Kathayat RS, Dickinson BC (2019) Activity-based sensing of S-depalmitoylases: chemical technologies and biological discovery. Acc Chem Res **52**: 3029–3038

Batistic O (2012) Genomics and localization of the Arabidopsis DHHC-cysteine-rich domain S-acyltransferase protein family. Plant Physiol **160**: 1597–1612

Burger M, Willige BC, Chory J (2017) A hydrophobic anchor mechanism defines a deacetylase family that suppresses host response against YopJ effectors. Nat Commun **8**: 2201

Cao Y, Qiu T, Kathayat RS, Azizi SA, Thorne AK, Ahn D, Fukata Y, Fukata M, Rice PA, Dickinson BC (2019) ABHD10 is an S-depalmitoylase affecting redox homeostasis through peroxiredoxin-5. Nat Chem Biol **15**: 1232–1240

Clough SJ, Bent AF (1998) Floral dip: a simplified method for Agrobacterium-mediated transformation of Arabidopsis thaliana. Plant J **16**: 735–743

De I, Sadhukhan S (2018) Emerging roles of DHHC-mediated protein S-palmitoylation in physiological and pathophysiological context. Eur J Cell Biol **97**: 319–338

Duan M, Zhang R, Zhu F, Zhang Z, Gou L, Wen J, Dong J, Wang T (2017) A lipid-anchored NAC transcription factor is translocated

into the nucleus and activates glyoxalase I expression during drought stress. Plant Cell **29**: 1748–1772

Feiguelman G, Fu Y, Yalovsky S (2018) ROP GTPases structure-function and signaling pathways. Plant Physiol **176**: 57–79

Hemsley PA (2020) S-acylation in plants: an expanding field. Biochem Soc Trans **48**: 529–536

Hemsley PA, Taylor L, Grierson CS (2008) Assaying protein palmitoylation in plants. Plant Methods **4**: 2

Hemsley PA, Weimar T, Lilley KS, Dupree P, Grierson CS (2013) A proteomic approach identifies many novel palmitoylated proteins in Arabidopsis. New Phytol **197**: 805–814

Hurst CH, Wright KM, Turnbull D, Leslie K, Jones S, Hemsley PA (2019) Juxta-membrane S-acylation of plant receptor-like kinases is likely fortuitous and does not necessarily impact upon function. Scient Rep **9**: 12818

Jiang H, Zhang X, Chen X, Aramsangtienchai P, Tong Z, Lin H (2018) Protein lipidation: occurrence, mechanisms, biological functions, and enabling technologies. Chem Rev **118**: 919–988

Koch E, Slusarenko A (1990) Arabidopsis is susceptible to infection by a downy mildew fungus. Plant Cell **2**: 437–445

Kumar S, Stecher G, Tamura K (2016) MEGA7: molecular evolutionary genetics analysis Version 7.0 for bigger datasets. Mol Biol Evol **33**: 1870–1874

Lai J, Yu B, Cao Z, Chen Y, Wu Q, Huang J, Yang C (2015) Two homologous protein S-acyltransferases, PAT13 and PAT14, cooperatively regulate leaf senescence in Arabidopsis. J Exp Bot **66**: 6345–6353

Lanyon-Hogg T, Faronato M, Serwa RA, Tate EW (2017) Dynamic protein acylation: new substrates, mechanisms, and drug targets. Trends Biochem Sci **42**: 566–581

Li H, Zeng R, Chen Z, Liu X, Cao Z, Xie Q, Yang C, Lai J (2018) S-acylation of a geminivirus C4 protein is essential for regulating the CLAVATA pathway in symptom determination. J Exp Bot **69**: 4459–4468

Li Y, Qi B (2017) Progress toward understanding protein S-acylation: prospective in plants. Front Plant Sci **8**: 346

Lin DT, Conibear E (2015a) ABHD17 proteins are novel protein depalmitoylases that regulate N-Ras palmitate turnover and subcellular localization. eLife **4**: e11306

Lin DT, Conibear E (2015b) Enzymatic protein depalmitoylation by acyl protein thioesterases. Biochem Soc Trans **43**: 193–198

Linder ME, Deschenes RJ (2007) Palmitoylation: policing protein stability and traffic. Nat Rev Mol Cell Biol **8**: 74–84

Liu L, Zhao Q, Xie Q (2012) In vivo ubiquitination assay by agroinfiltration. Methods Mol Biol **876**: 153–162

Mitchell DA, Vasudevan A, Linder ME, Deschenes RJ (2006) Protein palmitoylation by a family of DHHC protein S-acyltransferases. J Lipid Res **47**: 1118–1127

Qi D, Dubiella U, Kim SH, Sloss DI, Dowen RH, Dixon JE, Innes RW (2014) Recognition of the protein kinase AVRPPHB SUSCEPTIBLE1 by the disease resistance protein RESISTANCE TO PSEUDOMONAS SYRINGAE5 is dependent on s-acylation and an exposed loop in AVRPPHB SUSCEPTIBLE1. Plant Physiol **164**: 340–351

Qi Y, Tsuda K, Nguyen le V, Wang X, Lin J, Murphy AS, Glazebrook J, Thordal-Christensen H, Katagiri F (2011) Physical association of Arabidopsis hypersensitive induced reaction proteins (HIRs) with the immune receptor RPS2. J Biol Chem **286**: 31297–31307

Ranf S, Eschen-Lippold L, Frohlich K, Westphal L, Scheel D, Lee J (2014) Microbe-associated molecular pattern-induced calcium signaling requires the receptor-like cytoplasmic kinases, PBL1 and BIK1. BMC Plant Biol **14**: 374

Ren J, Wen L, Gao X, Jin C, Xue Y, Yao X (2008) CSS-Palm 2.0: an updated software for palmitoylation sites prediction. Protein Eng Des Select **21**: 639–644

Srivastava V, Weber JR, Malm E, Fouke BW, Bulone V (2016) Proteomic analysis of a poplar cell suspension culture suggests a major role of protein S-acylation in diverse cellular processes. Front Plant Sci **7**: 477

Swiderski MR, Innes RW (2001) The Arabidopsis PBS1 resistance gene encodes a member of a novel protein kinase subfamily. Plant J **26**: 101–112

Takemoto D, Jones DA (2005) Membrane release and destabilization of Arabidopsis RIN4 following cleavage by Pseudomonas syringae AvrRpt2. Mol Plant-Microbe Interact **18**: 1258–1268

Turnbull D, Hemsley PA (2017) Fats and function: protein lipid modifications in plant cell signalling. Curr Opin Plant Biol **40**: 63–70

Veronese P, Nakagami H, Bluhm B, Abuqamar S, Chen X, Salmeron J, Dietrich RA, Hirt H, Mengiste T (2006) The membrane-anchored BOTRYTIS-INDUCED KINASE1 plays distinct roles in Arabidopsis resistance to necrotrophic and biotrophic pathogens. Plant Cell **18**: 257–273

Wang Y, Lu H, Fang C, Xu J (2020) Palmitoylation as a signal for delivery. Adv Exp Med Biol **1248**: 399–424

Won SJ, Cheung See Kit M, Martin BR (2018) Protein depalmitoylases. Crit Rev Biochem Mol Biol **53**: 83–98

Yokoi N, Fukata Y, Sekiya A, Murakami T, Kobayashi K, Fukata M (2016) Identification of PSD-95 depalmitoylating enzymes. J Neurosci **36**: 6431–6444

Yoo SD, Cho YH, Sheen J (2007) Arabidopsis mesophyll protoplasts: a versatile cell system for transient gene expression analysis. Nat Protoc **2**: 1565–1572

Yuan X, Zhang S, Sun M, Liu S, Qi B, Li X (2013) Putative DHHC-cysteine-rich domain S-acyltransferase in plants. PLoS One **8**: e75985

Zaballa ME, van der Goot FG (2018) The molecular era of protein S-acylation: spotlight on structure, mechanisms, and dynamics. Crit Rev Biochem Mol Biol **53**: 420–451

Zhao G, Guo D, Wang L, Li H, Wang C, Guo X (2021) Functions of RPM1-interacting protein 4 in plant immunity. Planta **253**: 11

Zhou JM, Zhang Y (2020) Plant immunity: danger perception and signaling. Cell **181**: 978–989

Zhou L, Cheung MY, Li MW, Fu Y, Sun Z, Sun SM, Lam HM (2010) Rice hypersensitive induced reaction protein 1 (OsHIR1) associates with plasma membrane and triggers hypersensitive cell death. BMC Plant Biol **10**: 290

Zhou LZ, Li S, Feng QN, Zhang YL, Zhao X, Zeng YL, Wang H, Jiang L, Zhang Y (2013) Protein S-ACYL Transferase10 is critical for development and salt tolerance in Arabidopsis. Plant Cell **25**: 1093–1107

Zuo J, Niu QW, Chua NH (2000) Technical advance: an estrogen receptor-based transactivator XVE mediates highly inducible gene expression in transgenic plants. Plant J **24**: 265–273